New 2-methylimidazole–dicarboxylic acid molecular crystals: crystal structure and proton conductivity

2009 J. Phys.: Condens. Matter 21 345403

(http://iopscience.iop.org/0953-8984/21/34/345403)

J. Phys.: Condens. Matter **21** (2009) 345403 (9pp) doi:10.1088/0953-8984/21/34/345403

New 2-methylimidazole–dicarboxylic acid molecular crystals: crystal structure and proton conductivity

P Ławniczak[1], K Pogorzelec-Glaser[1], Cz Pawlaczyk[1], A Pietraszko[2] and L Szcześniak[1]

[1] Institute of Molecular Physics, Polish Academy of Sciences, Smoluchowskiego 17, 60-179 Poznań, Poland
[2] Institute of Low Temperatures and Structure Research, Polish Academy of Sciences, ulica Okólna 2, 50-422 Wrocław, Poland

E-mail: czpawl@ifmpan.poznan.pl

Received 16 March 2009, in final form 29 June 2009
Published 6 August 2009
Online at stacks.iop.org/JPhysCM/21/345403

Abstract

Three new proton conducting molecular crystals, 2-methylimidazole glutarate, 2-methylimidazole suberate and 2-methylimidazole azelate, were obtained and their structure was determined by the x-ray diffraction method. The structure of the crystals was found to be of layer-type. A hydrogen bond network between the heterocycle, glutaric acid and water molecules was apparent in a single layer of 2-methylimidazole glutarate, whereas chains consisting of two heterocyclic molecules linked with hydrogen bonds with dicarboxylic acid were distinguished in a single layer of 2-methylimidazole suberate and azelate crystals. Thermal stability of the crystals was characterized by differential scanning calorimetry and the electrical conductivity was studied by the impedance spectroscopy method. The maximum conductivity of 2-methylimidazole glutarate pellets amounts to 3.3×10^{-2} S m^{-1} at 325 K, in the case of 2-methylimidazole suberate pellets the maximum conductivity is 2.4×10^{-4} S m^{-1} at 348 K and for 2-methylimidazole azelate pellets the maximum conductivity reaches 6.9×10^{-4} S m^{-1} at 353 K.

(Some figures in this article are in colour only in the electronic version)

1. Introduction

During the last decade political, economical and environmental protection aspects stimulated research activity into polymer electrolyte fuel cells (PEFCs). As the behavior of the electrolyte membrane determines the PEFC performance the search for new electrolyte membranes conductive under anhydrous conditions drew attention to the properties of nitrogen-containing heterocyclic molecules [1–5]. Such heterocycles as imidazole, pyrazole, 1-methylimidazole and benzimidazole immobilized in a polymer membrane in a way that enables high proton mobility are interesting PEFC materials since, similar to water, they exhibit the ability to form a hydrogen bond network. The conduction mechanism in polymer-immobilized heterocycles is of Grotthuss type and the structure diffusion proceeds via reorientation of adjacent heterocyclic molecules and reorganization of the coordination sphere of the migrating protons [6]. Various approaches have been used to immobilize the heterocyclic molecules in polymer membranes. A direct bonding of the imidazole moieties to the polymer backbone in the form of poly(4-vinylimidazole) resulted in a rather low conductivity [7]. Another possibility is the immobilization of the heterocycles via flexible spacers: imidazole-terminated ethyleneoxide oligomers [1, 3], imidazole- and 1-methylimidazole-terminated ethyleneoxide oligomers doped with strong acid [5], as well as polystyrene with imidazole-terminated flexible side chains and benzimidazole bonded to an SiO_2 network by a flexible spacer [4]. Anhydrous proton-conducting membranes were also prepared from imidazole, pyrazole, 1-methylimidazole and benzimidazole with poly(vinylphosphonic acid) [8, 9]. An interesting attempt to combine imidazole with biopolymers such as chitin

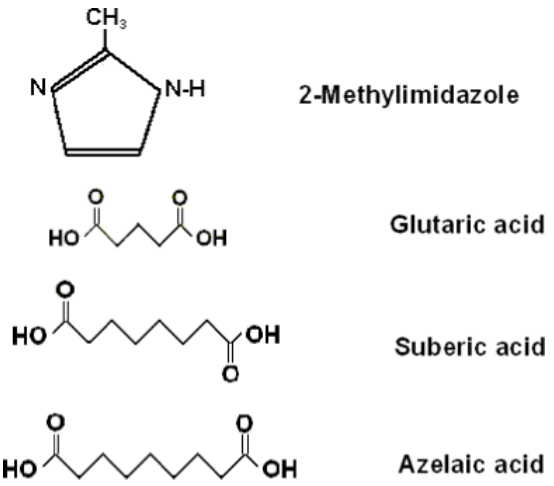

Figure 1. Molecules of 2-methylimidazole, glutaric acid, suberic acid and azelaic acid.

phosphate and alginic acid was proposed [9, 10]. Moreover, acid-doped polybenzimidazole membranes and blends of polybenzimidazole and sulfonated polysulfones were used as polymer electrolytes [11–13].

We were interested in the structure and electrical conductivity of imidazole complexes/salts with dicarboxylic acids and analyzed the hydrogen bond network which can enable the structural diffusion [14–17]. In this paper we report the results of a hydrogen network and proton conductivity study of dicarboxylic acid salts with 2-methylimidazole, a molecule with dipole moment very similar to that of imidazole but of different steric hindrance due to the dynamics of the CH_3 group. Three new salts, 2-methylimidazole glutarate (2-MIm GLU), 2-methylimidazole suberate (2-MIm SUB) and 2-methylimidazole azelate (2-MIm AZL) (the substrate molecules are shown in figure 1), were obtained and their structure was solved.

2. Experimental details

2.1. Synthesis, crystallization and sample preparation

2-methylimidazole (Fluka, purity $\geqslant$98.0%) and the respective dicarboxylic acid (glutaric, suberic, azelaic acid, Aldrich 98.0%) were dissolved separately in acetone (Aldrich, pro analysis) at room temperature. The obtained substrate solutions were mixed together and stirred at 310 K until a white precipitate disappeared. The crystallization of the salts was carried out by slow evaporating of the solvent at room temperature and needle-like crystallites 4 mm in length and about 0.3 mm thick were obtained. The single crystals were used in an XRD study of the structure and thermal analysis. For conductivity measurements pellets 1.5 mm thick and 13 mm in diameter were made from powder obtained by 30 min milling of the crystals in an agate mortar. The powder was pressed under 30 MPa for 1 min at room temperature in the form of pellets, the surfaces of which were electroded with Hans Wolbring GmbH silver paste.

2.2. Thermal analysis

Thermal stability of the complexes of 2-methylimidazole with glutaric, suberic and azelaic acid was studied by means of differential scanning calorimetry (DSC). DSC data were obtained with a Netzsch DCS 200 calorimeter in the temperature range 300–380 K. The measurements were carried out both on heating and cooling and the temperature was changed at a rate of 5 K min^{-1}.

2.3. X-ray measurements

Single-crystal x-ray diffraction measurements were done with an x-ray four-circle XCALIBUR Diffractometer (Oxford Diffraction Company) with a CCD area detector at 298 K and at low temperatures using a low temperature attachment (Oxford Cryo-System 1998). Graphite-monochromated Mo Kα radiation (0.7107 Å) was generated at 50 kV and 25 mA. The unit cell was indexed from all the frames and positional data were refined with diffractometer constants to yield the final cell parameters. Integration and scaling correction, performed with the CrysAlis program version 172.32.18 OXFORD DIFFRACTION, resulted in the unique datasets corrected for Lorentz polarization effects. The same CrysAlis program was used to introduce the absorption corrections. The structures were solved using the SHELXS97 program [18] and refined using the full-matrix least-squares methods in the program. The CIF files with the crystal structure data have been sent as a deposit in the CSD database.

2.4. Conductivity measurements

The real and imaginary parts of electric impedance of complexes of 2-methylimidazole with glutaric, suberic and azelaic were studied in the frequency range from 100 Hz to 13 MHz by means of a computer-controlled HP-4192A impedance analyzer. The temperature of the sample was stabilized to within 0.05 K using a CF 1204 Oxford Instruments cryostat, equipped with an ITC 4 temperature controller.

3. Results and discussion

3.1. The crystal structure

The results of the XRD studies of 2-methylimidazole salts with glutaric, suberic and azelaic acids at low temperatures are collected in table 1. The H atoms of 2-methylimidazole and carboxylic acid molecules were located from the difference Fourier map and their positional parameters were refined freely, however, with an isotropic displacement parameter 1.2 times that of the neighboring N or O atoms.

3.1.1. The crystal structure of 2-methylimidazole glutarate. The 2-MIm GLU crystallizes in a triclinic system with centrosymmetric $P\bar{1}$ space group. The moiety formula per unit cell of the 2-MIm-glutarate crystal is as follows: $2(C_5H_7O_4)^-$, $2(C_5H_6O_4)^{2-}$, $5(C_4H_7N_2)^+$, $(C_8H_{13}N_4)^+$ and $4(H_2O)$. The crystal structure is of layer-type (figure 2(a)) with layers parallel to the $(\bar{2}\bar{1}1)$ plane (figure 2(b)).

Table 1. Low temperature crystal structure data of 2-methylimidazole glutarate (2-MIm GLU), 2-methylimidazole suberate (2-MIm SUB) and 2-methylimidazole azelate (2-MIm AZL).

Data	2-MIm GLU	2-MIm-SUB	2-MIm-AZL
Empirical formula	C24 H41 N7 O10	C16 H26 N4 O4	C51 H84 N12 O12
Formula weight	587.64	338.41	1057.30
Temperature (K)	140(2)	110(2)	150(2)
Wavelength (Å)	0.710 73	0.710 73	0.710 73
Cryst. system/space group	Triclinic, $P\bar{1}$	Monoclinic, $P2(1)/n$	Monoclinic, $C2/c$
a (Å)	7.0789(7)	11.299(2)	22.682(5)
b (Å)	10.5908(8)	13.797(3)	11.577(2)
c (Å)	20.3403(15)	11.797(2)	22.930(5)
alpha (deg)	96.632(6)	90	90
beta (deg)	94.377(7)	109.12(3)	110.49(3)
gamma (deg)	99.013(7)	90	90
Volume (A^3)	1489.1(2)	1737.6(6)	5640.2(19)
Z, calculated density (Mg m^{-3})	2, 1.311	4, 1.294	4, 1.245
Absorption coefficient (mm^{-1})	0.103	0.094	0.090
$F(000)$	628	728	2280
Crystal size (mm × mm × mm)	0.32 × 0.28 × 0.18	0.38 × 0.31 × 0.23	0.32 × 0.25 × 0.21
Theta range at collec. (deg)	4.18–27.47	3.47–28.15	3.75–27.09
Limiting indices	$-9 \leqslant h \leqslant 8$, $-13 \leqslant k \leqslant 13$, $-25 \leqslant l \leqslant 26$	$-15 \leqslant h \leqslant 14$, $-18 \leqslant k \leqslant 17$, $-13 \leqslant l \leqslant 15$	$-28 \leqslant h \leqslant 28$, $-12 \leqslant k \leqslant 14$, $-29 \leqslant l \leqslant 29$
Reflections collec./uniq.	18 265/6707[R(int) − 0.0282]	16 732/4004[R(int) − 0.0208]	25 032/6005[R(int) − 0.0471]
Completeness.-theta (%)	98.2	94.2	96.5
Max.–min. transmission	0.9958 and 0.9674	0.9822 and 0.9712	0.9921 and 0.9751
Data/restrain./paramet.	6707/5/544	4004/0/321	6005/0/515
Goodness-of-fit on F^2	1.083	0.992	1.273
Final-R-indic. ($I > 2$sigma(I))	$R1 = 0.0434$, $wR2 = 0.0796$	$R1 = 0.0357$, $wR2 = 0.0820$	$R1 = 0.0685$, $wR2 = 0.1269$
R indices (all data)	$R1 = 0.0719$, $wR2 = 0.0845$	$R1 = 0.0517$, $wR2 = 0.0874$	$R1 = 0.1028$, $wR2 = 0.1366$

A single layer comprises planar 2-methylimidazole molecules and almost planar glutaric acid molecules. In the layer the molecules are linked into a two-dimensional framework by hydrogen bonds of three types (figure 3).

The O–H···O hydrogen bonds are formed by $[(C_5H_7O_4)^-(C_5H_6O_4)]$ and $[(H_2O)–(H_2O)]$ molecules, the N–H···O hydrogen bonds are between the $[(C_4H_7N_2)–(C_5H_7O_4)]$ molecules, $[(C_4H_7N_2)–(H_2O)]$ molecules and $[(C_8H_{13}N_4)–(C_5H_7O_4)]$ molecules, whereas the N–H···N hydrogen bonds are linking only two $[(C_4H_7N_2)–(C_4H_6N_2)]$ molecules. The details of the hydrogen bonds are presented in table 2.

The layers are stacked into a three-dimensional structure and linked with a weak π–π interaction between imidazole rings in neighboring layers. It should be observed that the packing of the molecules into layers in the centrosymmetric triclinic space group $P\bar{1}$ results in a disorder of one of the 2-methylimidazole molecule denoted as (F) in figure 3.

3.1.2. The crystal structure of 2-methylimidazole suberate. The crystal structure of 2-MIm SUB belongs to a monoclinic system with $P2_1/n$ space group. The architecture of the crystal structure is also of layer-type with layers parallel to the (010) plane (figure 4(a)). The layers are formed by chains of planar suberic acid molecules and $[(C_4H_7N_2)–(C_4H_6N_2)]$ groups (figure 4(b)).

The heterocyclic molecules are joined together with N–H···N hydrogen bonds and linked by N–H···O bonds with the acid molecules. The acid chains are parallel to the c axis and joined by the strong O–H···O type hydrogen bonds (table 3). All the hydrogen bonds form a two-dimensional network in the layers. The layers are linked by weak interactions of C–H···π type between the imidazole rings and the methyl groups.

3.1.3. The crystal structure of 2-methylimidazole azelate. The 2-MIm-AZL crystal has $[2(C_4H_7N_2)^{+1}(C_4H_6N_2)–2(C_5H_7O_4)^-]$ chemical structure and crystallizes in a monoclinic system with $C2/c$ space group. The packing of the 2-methylimidazole and azelaic acid molecules in the crystal forms layers parallel to the (100) plane (figure 5) and the details of the structure differs from those of the 2-MIm SUB compound.

In each layer one can distinguish ribbons made of $[(C_4H_7N_2)–(C_4H_6N_2)]$ groups linked by N–H···N bonds. The ribbons are joined with azelaic acid by moderate N–H···O bonds. The acid molecules in the ribbon are oriented along the c axis and linked with strong O–H···O hydrogen bonds lying primarily along the b direction (figure 6(a)).

The interactions between the ribbons in a single layer are of C–H···.O type. The three-dimensional structure comprises two symmetrically non-equivalent layers. The layers located in the positions $x = 0$ and 0.5 contain an inversion symmetry operation. A disorder of protons in the N–H···N hydrogen bonds linking two 2-methylimidazole molecules as well that of protons in the O–H···O bonds between the acid molecules

Table 2. Hydrogen bonds in the crystal structure of 2-MIm-GLU (see figure 3).

D–H · · · A	*d* (D–H) (Å)	*d* (H · · · A) (Å)	*d* (D · · · A) (Å)	<(DHA) (deg)
O(1B)–H(1B) · · · O(4A)	0.970(7)	1.602(7)	2.5714(5)	178.2(7)
N(1C)–H(1C) · · · O(4B)#2	0.900(5)	1.816(5)	2.7019(6)	167.8(4)
N(3C)–H(3C) · · · O(4A)#3	0.944(5)	1.785(5)	2.7211(5)	170.8(5)
N(3C)–H(3C) · · · O(3A)#3	0.944(5)	2.569(5)	3.2697(5)	131.3(4)
N(1E)–H(1E) · · · O(2A)#4	0.973(6)	1.663(6)	2.6196(5)	166.5(6)
N(1D)–H(1D) · · · OH1#5	0.905(5)	1.829(5)	2.7310(6)	174.2(5)
N(3D)–H(3D) · · · N(3D)#6	0.860(8)	1.788(8)	2.6474(9)	177.9(11)
N(3E)–H(3E) · · · O(3B)#2	0.952(6)	1.739(5)	2.6666(5)	163.9(5)
OH1–H(11) · · · O(2A)	0.901(6)	1.822(6)	2.7232(5)	179.6(6)
OH2–H(21) · · · O(3B)#7	0.896(6)	1.883(6)	2.7665(5)	168.8(6)
OH1–H(12) · · · OH2#3	0.865(6)	1.930(6)	2.7834(5)	168.8(6)
OH2–H(22) · · · O(3A)	0.963(7)	1.816(7)	2.7742(6)	173.3(6)
N(1F)–H(1F) · · · O(1A)	0.94	1.74	2.666(11)	167.3

Table 3. Hydrogen bonds in the 2-MIm SUB crystal structure.

D–H · · · A	*d* (D–H) (Å)	*d* (H · · · A) (Å)	*d* (D · · · A) (Å)	<(DHA) (deg)
N(3A)–H(3A) · · · O(3)#1	0.950(4)	1.933(5)	2.8743(11)	170.6(5)
N(1B)–H(1B) · · · N(1A)#2	1.051(6)	1.640(6)	2.6884(7)	174.7(5)
N(3B)–H(3B) · · · O(1)	0.991(5)	1.737(5)	2.7239(10)	173.3(6)
O(4)–H(4) · · · O(2)#3	1.076(6)	1.404(6)	2.4788(7)	176.1(6)

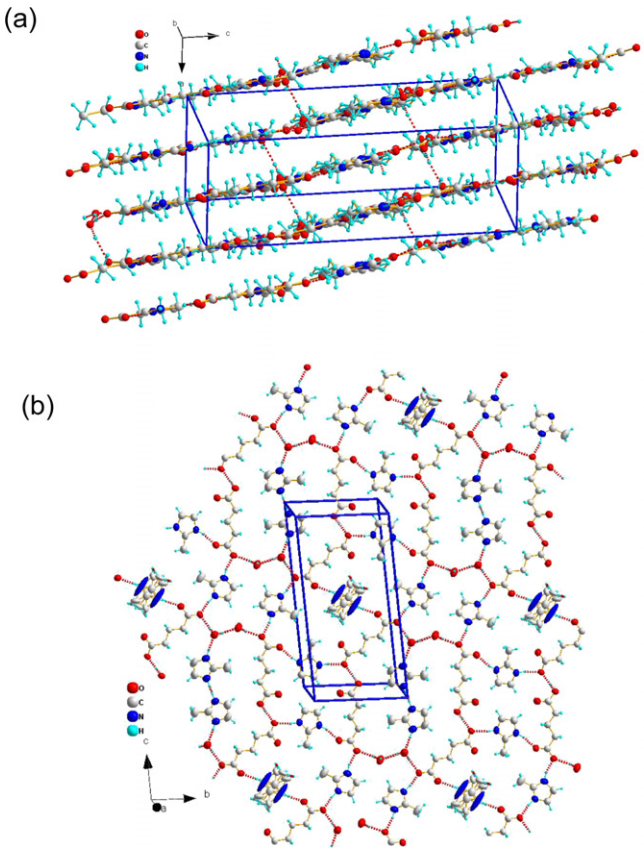

Figure 2. The crystal structure of 2-MIm GLU: projection onto the $(\bar{1}\ \bar{1}\ 0\ 0)$ plane (a) and projection of a single layer onto the $(\bar{2}\ \bar{1}\ 1)$ plane (b).

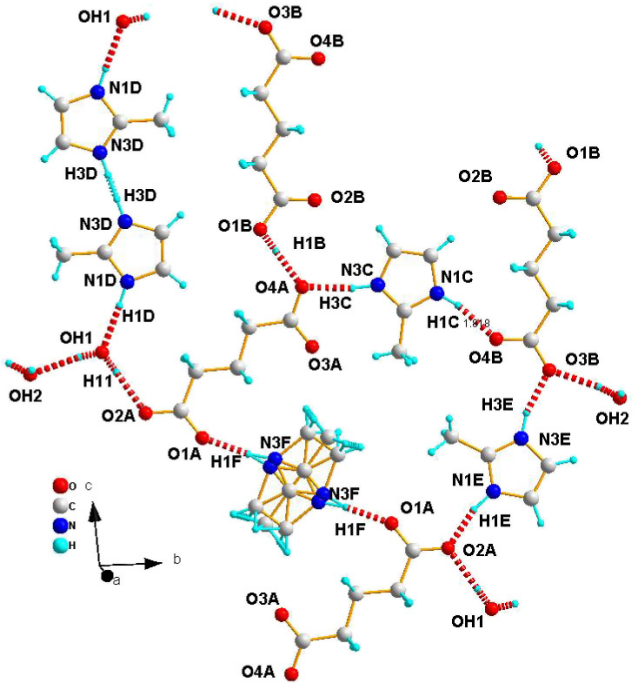

Figure 3. Part of a single layer of 2-MIm GLU structure, showing the formation of hydrogen bonds. The H bonds to N and O atoms are marked by thick dashed lines.

is related to the twofold axis operation and the inversion operation, respectively (figure 6(b)). It should be observed, however, that protons in the other hydrogen bonds lying in a layer are ordered (figure 6(a)). The details of the hydrogen bonds in the 2-MIm azelaic acid compound are presented in table 4.

3.1.4. Proton transfer in 2-MIm carboxylic acid molecular crystals. The 2-methylimidazole molecules, like other nitrogen-containing heterocycles (imidazole, triazole and benzimidazole), are known to crystallize in layer crystal

Table 4. Hydrogen bonds in the 2-MIm AZL crystal structure.

D–H · · · A	*d* (D–H) (Å)	*d* (H · · · A) (Å)	*d* (D · · · A) (Å)	<(DHA) (deg)
N(3C)–H(3C) · · · O(1A)	0.885(6)	1.932(7)	2.8108(9)	171.4(6)
N(3D)–H(3D) · · · O(3A)#2	0.908(9)	1.807(9)	2.7138(9)	175.5(8)
N(3E)–H(3E) · · · O(2B)	0.816(8)	1.959(8)	2.7730(10)	175.9(8)
N(1D)–H(1D) · · · N(1C)#3	1.057(10)	1.690(10)	2.7388(10)	171.1(8)
N(1E)–H(1E) · · · N(1E)#4	1.007(19)	1.723(17)	2.7005(13)	162.4(18)

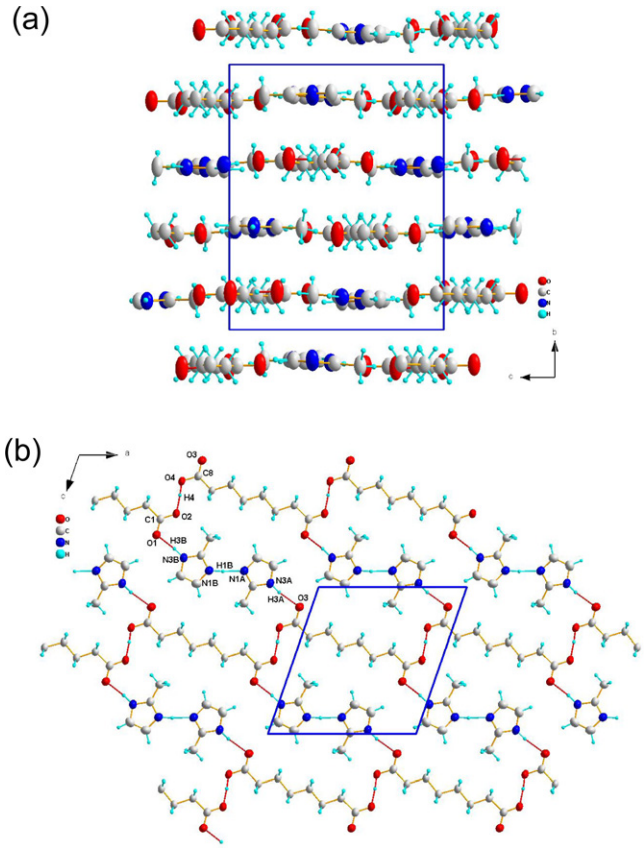

Figure 4. Layer structure of 2-MIm SUB: packing of the layers along the *a* monoclinic axis (a); arrangement of suberic acid molecules and 2-methylimidazole molecules in the layer (b).

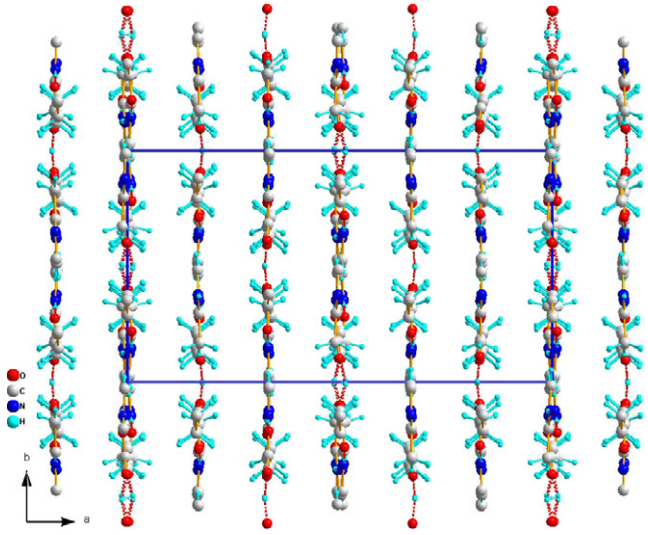

Figure 5. Projection of the crystal structure of 2-MIm AZL along the *c* monoclinic axis.

structures held together by a hydrogen bond network, where the protons can easily migrate. The proton transfer in 2-MIm carboxylic acid molecular crystals is closely related to the layer crystal structure. A possible diffusion pathway within a layer, in the frame of the Grotthuss mechanism, will comprise proton hops which couple to the charged defects and rotational modes of 2-MIm molecules. An example of possible trajectories of proton transfer in the 2-MIm SUB crystal is shown in figure 7.

3.2. Thermal stability

DSC scans on heating and cooling 2-methylimidazole glutarate, suberate and azelate crystals in the temperature range 300–380 K are shown in figure 8.

Irreversible changes are observed on heating the 2-MIm GLU crystal to 380 K because the hydrate loses the water of crystallization. The dehydration process is rather complex and the analysis of the DSC spectrum using a Fraser–Suzuki function yields four endothermic processes with peaks at 341, 357, 366a nd 360 K and respective enthalpies of 13.5, 36.5, 20.0 and 46.5 J g^{-1}. On cooling from 380 K a single DSC anomaly appears with an onset at ∼343 K, endset at ∼317 K and maximum at 330 K with the enthalpy of 74.0 J g^{-1}. In the case of 2-MIm SUB and 2-MIm AZL crystals, which do not contain the water of crystallization in their crystal lattice, melting and crystallization processes are apparent in the heating and cooling DSC scans. The onset of the melting process of 2-MIm SUB is visible at ∼348 K and the maximum melting rate occurs at 358 K, whereas the crystallization process starts at ∼345 K and the maximum rate is observed at 333 K. The melting onset temperature of 2-MIm AZL is ∼346 K and the maximum melting rate is observed at 364 K, whereas the crystallization onset appears at ∼339 K with the maximum rate at 324 K. The melting enthalpies of the suberate and azelate crystals are similar and equal to 162 J g^{-1}, whereas the enthalpies related to the crystallization process amount to −135 J g^{-1} and −150 J g^{-1} for 2-MIm SUB and 2-MIm AZL.

3.3. Electrical conductivity

Temperature variation of the electrical conductivity σ of the dicarboxylic acid salts of 2-methylimidazole was obtained from the measurement of the complex impedance of the pellets at constant temperatures in the frequency range between 100 Hz and 13 MHz. Examples of the Nyquist plots (i.e. the

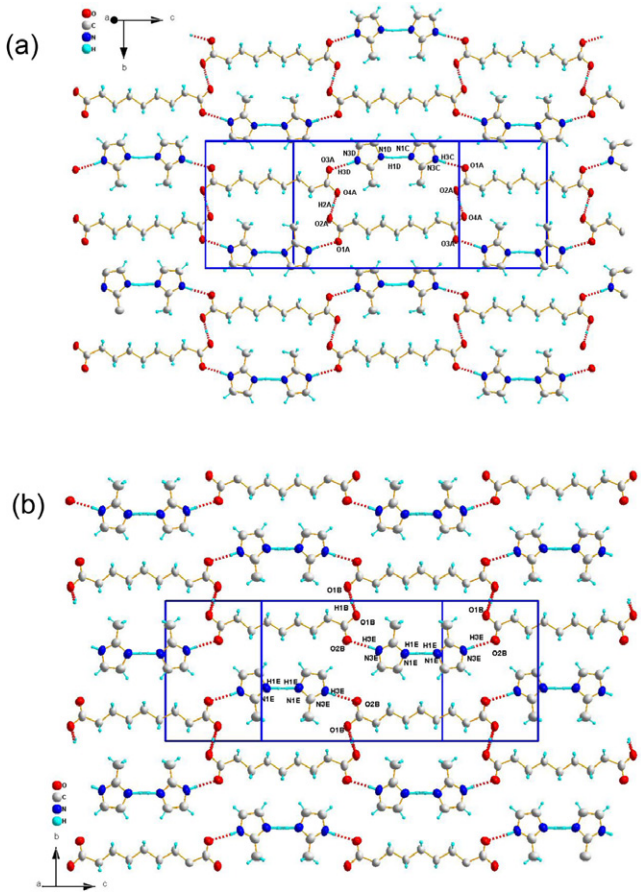

Figure 6. Arrangement of 2-methylimidazole and azelaic acid molecules in the (100) plane: (a) at $x = 0$ and (b) at $x = 0.5$.

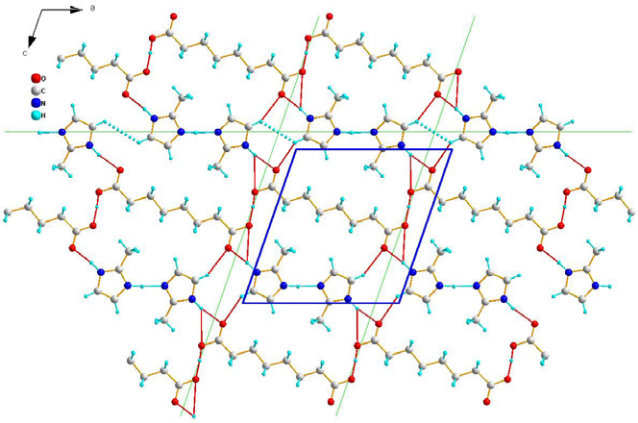

Figure 7. Projection of a layer of 2-MIm SUB crystal with marked lines of possible trajectories of proton transport.

dependence of the imaginary part Z'' of the impedance on the real part Z') at various temperatures are shown in figure 9.

It can be observed that the experimental points lie on flattened semicircles originating in the beginning of the (Z'', Z') coordinate system, which points to a heterogeneity of the samples. The flattening of the semicircles, indicating a distribution of the time constants, may be related to the fact that the samples are composed of small crystallites of different size pressed together.

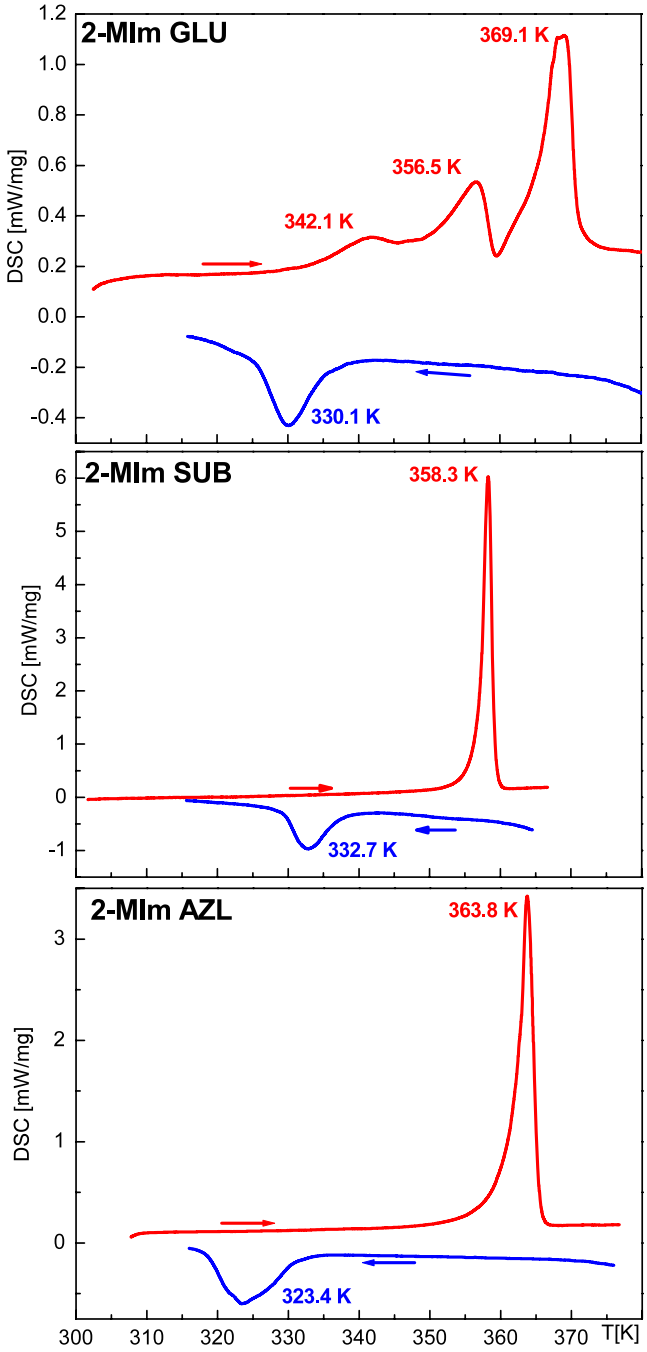

Figure 8. DSC scans of 2-MIm GLU, 2-MIm SUB and 2-MIm AZL molecular crystals; $dT/dt = 5$ K min^{-1}.

In the case of 2-MIm GLU salt the impedance response at lower temperatures is clearly composed of two semicircles, which can be attributed to two processes. As has been shown in section 3.1 the structure of the glutaric acid salt of 2-methylimidazole differs considerably from those of suberic and azelaic acids because it contains the water of crystallization. In the structure of 2-Mim GLU there are two types of hydrogen bonds: O–H $\cdots$ O between water molecules and the N–H $\cdots$ O between ($C_4H_7N_2$) and water molecules, which are not present in the two other structures. It suggests that an additional conduction path for the charge carriers in 2-MIm GLU, giving

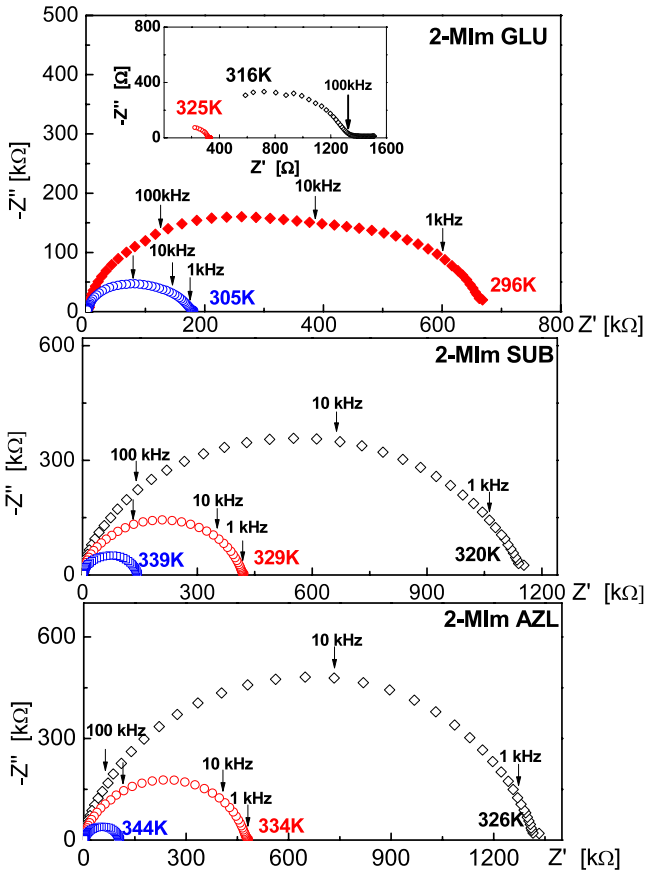

Figure 9. Examples of complex impedance plots for 2-MIm GLU, 2-MIm SUB and 2-MIm AZL.

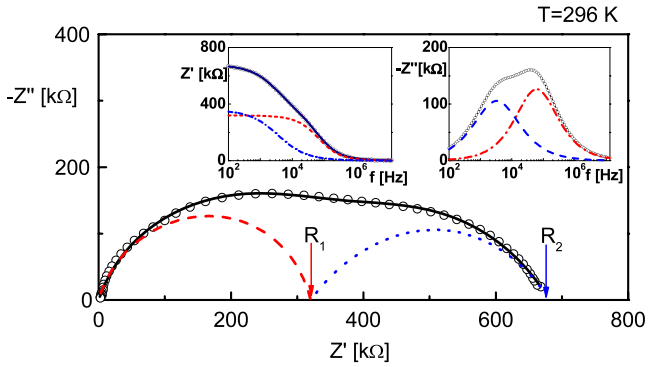

Figure 10. An example of the fit (solid and dashed lines) of the experimental data (open circles) for 2-MIm GLU at 296 K using the formula (1).

an additional contribution to the total conductivity, is possible. In such a case double RC parallel equivalent circuits connected in series should be used for fitting the experimental data. The double contribution response was, however, observed only at temperatures up to 307 K. Above this temperature the conductivity increases rapidly and in the frequency range available in our experiment only a part of the impedance spectrum could be measured, as has been shown in the inset in figure 9(a). In the temperature range between 307 K and the melting point the impedance response seems to have one contribution only.

At lower temperatures the separation of both contributions is possible and an example of the fit to the impedance data measured at the temperature of 296 K is shown in figure 10. The situation is then similar to that found, for example, for n-type phosphorus-doped diamond [19] where two well-separated semicircular responses above 75 °C were observed, suggesting the presence of two conduction paths with various activation energies. Similarly, in the case of nanostructured diamond films [20] the impedance spectroscopy enabled us to reveal two contributions to the electrical conductivity: from grain interior and from grain boundaries, each of them dominating in different temperature regions. In general, combining temperature changes and impedance spectroscopy measurements, often more than one (multiple) conduction mechanism can be shown to exist [21, 22]. For fits as in figure 10 the Cole–Cole formula for double RC parallel equivalent circuits connected in series was used:

$$Z(\omega) = Z' - \mathrm{j}Z'' = \frac{R_1}{1 + (\mathrm{j}\omega R_1 C_1)^{1-\alpha_1}} + \frac{R_2 - R_1}{1 + (\mathrm{j}\omega (R_2 - R_1) C_2)^{1-\alpha_2}}, \quad (1)$$

where R_1 denotes the resistance of the first contribution, R_2—the resistance of the sum of both contributions, C_1 and C_2—electrical capacities of circuits 1 and 2, α_1 and α_2—Cole–Cole parameters and $\omega = 2\pi f$—the angular frequency of the measuring field. It is worth noting that the fit should be done for both dependences $Z'(f)$ and $Z''(f)$ separately (see the inset in figure 10).

Frequency dependences of the real part of the conductivity $\sigma'(f)$ of dicarboxylic salts of 2-methylimidazole at various temperatures are shown in figure 11.

From the low-frequency plateau of the $\sigma'(f)$ curves in the case of 2-MIm SUB and 2-Mim AZL or from the fits as in figure 10 for 2-MIm GLU one can determine the dc conductivity of the samples at given temperatures. The dc conductivity of the salts versus the inverse temperature is presented in figure 12.

The dc conductivity of the three salts can be described by the Arrhenius law:

$$\sigma(T) = \sigma_0 \exp(-E_a/kT),$$

with σ_0 denoting the pre-exponential factor, E_a the activation energy and k the Boltzmann constant. The observed deviations from the Arrhenius behavior at higher temperatures are related to the thermal decomposition in the case of the glutaric acid salt and to the initial melting stage of the sample of the suberic and azelaic acid salts. The activation energies of 2-MIm GLU, calculated from the linear part of the $\log \sigma_{dc}(1/T)$ dependence (where the fit with double parallel circuits was possible), amount to $E_a = 1.12$ eV when taken from R_1 and E_a =1.05 eV when taken from R_2 and are comparable to the activation energies $E_a = 1.1$ eV and $E_a = 1.5$ eV of 2-methylimidazole suberate and azelate, respectively. The maximum conductivity of the hydrated salt of 2-methylimidazole amounts to σ =

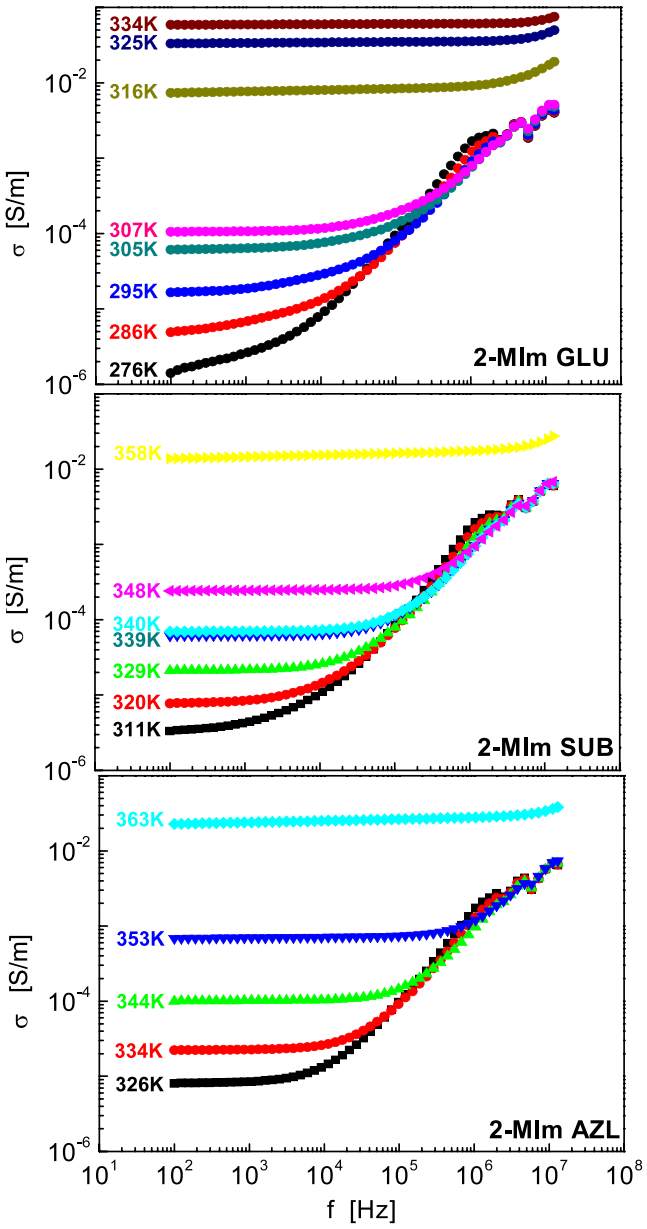

Figure 11. Frequency dependence of the real part of the ac conductivity of 2-MIm GLU, 2-MIm SUB and 2-MIm AZL.

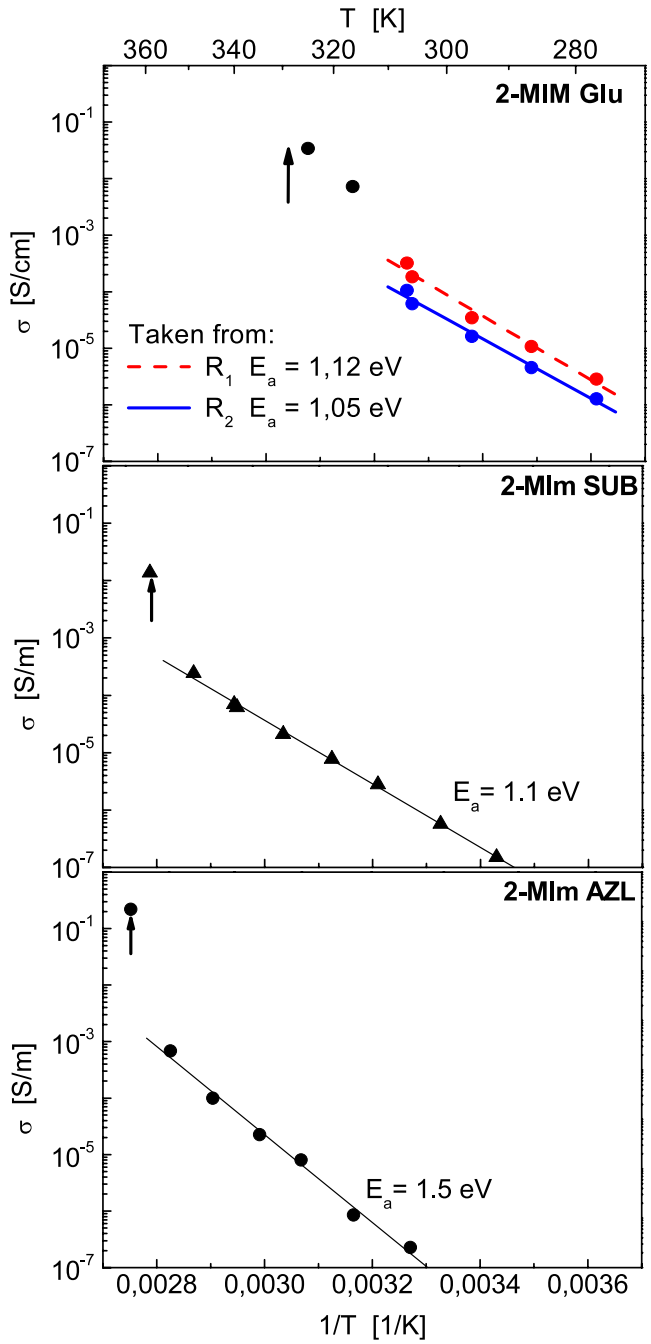

Figure 12. Arrhenius plots of dc conductivity of 2-MIm GLU, 2-MIm SUB and 2-MIm AZL (arrows point at melting temperatures).

0.033 S m^{-1} at 325 K and is considerably higher in comparison with those of the non-hydrated salts probably due to the contribution of the dynamics of the water of hydration.

Both the imidazole and 2-methylimidazole salts of dicarboxylic acids form a well-defined layer structure. Unfortunately, we were not able to grow sufficiently large crystals to measure the anisotropy of the conductivity. Earlier studies of the pellets made of imidazole salts of dicarboxylic acids showed that the activation energy of the conductivity increases with the length of the acid chain [14, 16]. We have observed the same effect for the salts of 2-methylimidazole. The conductivity values close to the melting point of the imidazole salts are higher than those of the 2-methylimidazole crystals. Because the dipole moments of the two types of heterocycles are very similar, the concentration of protons available for conduction in the salts should be dependent on their basicity. Indeed, the self-dissociation process of imidazole has been found to be more efficient than that of 2-methylimidazole [23]. The respective pK_a values of the dissociation process of imidazole-type heterocycles I:

$$IH^+ \overset{K_1}{\longleftrightarrow} I \overset{K_2}{\longleftrightarrow} I^-$$

are $pK_1 = 6.95$ and $pK_2 = 13.96$ for imidazole and $pK_1 = 7.75$ and $pK_2 = 14.72$ for 2-methylimidazole [23].

4. Conclusions

This work aimed at determining the effect of the structure of five-membered nitrogen-containing heterocyclic molecules on the hydrogen bond network and proton conductivity of salts of dicarboxylic acids. We studied the effect in salts of 2-methylimidazole with glutaric, suberic and azelaic acids. The dipole moment of the 2-methylimidazole molecule calculated with the PM3 method using the 9.034 version of MOPAC2009 amounts to 3.80 D and is very close to the dipole moment value of 3.86 D obtained for the 1H-imidazole molecule but the steric hindrance of both molecules differs due to the CH_3 group dynamics.

The studied molecular crystals of 2-methylimidazole of dicarboxylic acids were found to form layer-type structures similar to the case of the imidazole compounds [14–17]. It should be noted, however, that a two-dimensional hydrogen bond network is apparent in a single layer of 2-MIm GLU and 2-MIm-SUB crystals but in the case of 2-MIm AZL crystals the hydrogen bond network was observed only in the ribbons parallel to the *c* monoclinic axis. In all the crystals studied one can distinguish two 2-methylimidazole molecules linked by N–H $\cdots$ N bonds forming $[(C_4H_7N_2)$–$(C_4H_6N_2)]$ groups. In the 2-MIm GLU crystal structure, however, the layers also comprise single 2-methylimidazole molecules and H_2O molecules. As the crystal structure of 2-MIm GLU, 2-MIm SUB and 2-MIm AZL is of a layer type a strong anisotropy of electrical conductivity is to be expected. Unfortunately, we were not able to grow sufficiently large crystals to study the anisotropy and the studies of electrical conductivity of the pressed pellets of the materials yielded only information on the average conductivity and the activation energy. The highest conductivity was observed for the 2-MIm GLU crystals and we relate it to the contribution of the hydration water dynamics. The 2-methylimidazole salts were found to exhibit lower conductivity values below the melting point (in 2-MIm GLU before dehydration) than corresponding imidazole salts [14, 16]. This may be related to higher efficiency of the self-dissociation of imidazole in comparison with that of 2-methylimidazole. The activation energy of the conductivity was found to increase with the chain length of the dicarboxylic acids, similarly as it has been reported in the case of the imidazole dicarboxylic acid salts.

Acknowledgments

The authors are indebted to Professor Jerzy Małecki for the dipole moment calculations.

This work was supported by the Ministry of Science and Higher Education in Poland, grant no. N N507 3852 33.

References

[1] Kreuer K D 2001 *J. Membr. Sci.* **185** 29
[2] Kreuer K D, Fuchs A, Ise M, Spaeth M and Maier J 1998 *Electrochim. Acta* **43** 1281
[3] Schuster M, Meyer W H, Wegner G, Herz H G, Ise M, Schuster M, Kreuer K D and Maier J 2001 *Solid State Ion.* **145** 85
[4] Herz K G, Kreuer K D, Maier J, Scharfenberger G, Schuster M F H and Meyer W H 2003 *Electrochim. Acta* **48** 2165
[5] Schuster M F H, Meyer W H, Schuster M and Kreuer K D 2004 *Chem. Mater.* **16** 329
[6] Münch W, Kreuer K D, Silvestri W, Maier J and Seifert G 2001 *Solid State Ion.* **145** 437
[7] Bozkurt A and Meyer W H 2001 *Solid State Ion.* **138** 85
[8] Yamada M and Honna I 2005 *Polymer* **46** 2986
[9] Honna I and Yamada M 2007 *Bull. Chem. Soc. Japan* **80** 2110
[10] Yamada M and Honna I 2004 *Polymer* **45** 8349
[11] Wang J-T, Savinell R F, Wairight J, Litt M and Yu H 1996 *Electrochim. Acta* **41** 193
[12] Bouchet R, Miller S, Duclot M and Souquet S L 2001 *Solid State Ion.* **145** 69
[13] Hasistis C, Demede V and Kontoyannis C 2001 *Electrochim. Acta* **46** 2401
[14] Pogorzelec-Glaser K 2005 *PhD Thesis* Poznań University of Technology
[15] Garbarczyk J and Pogorzelec-Glaser K 2003 *Z. Kristallogr.* **218** 567
[16] Pogorzelec-Glaser K, Pawlaczyk Cz, Garbarczyk J and Markiewicz E 2006 *Mater. Sci. Pol.* **24** 245
[17] Pogorzelec-Glaser K, Pawlaczyk Cz, Pietraszko A and Markiewicz E 2007 *J. Power Sources* **173** 800
[18] Sheldrick G M 2008 *Acta Crystallogr.* A **64** 112
[19] Curat S, Ye H, Gaudin O and Jackman R B 2005 *J. Appl. Phys.* **98** 073701
[20] Ye H, Sun C Q, Huang H and Hing P 2001 *Appl. Phys. Lett.* **78** 1826
[21] Tumilty N, Welch J, Ye H, Balmer R S, Wort C, Lang R and Jackman R B 2009 *Appl. Phys. Lett.* **94** 05210
[22] Bevilacqua M, Patel S, Chaudhary A, Ye H and Jackman R B 2008 *Appl. Phys. Lett.* **93** 132115
[23] Bruice T C and Schmir G L 1958 *J. Am. Chem. Soc.* **80** 148